Hypomorphic mutation of PGC-1β causes mitochondrial dysfunction and liver insulin resistance

Claudia R. Vianna,[1,8] Michael Huntgeburth,[1,2,8] Roberto Coppari,[1,9] Cheol Soo Choi,[3] Jiandie Lin,[6] Stefan Krauss,[1] Giorgio Barbatelli,[7] Iphigenia Tzameli,[1] Young-Bum Kim,[1] Saverio Cinti,[7] Gerald I. Shulman,[3,4,5] Bruce M. Spiegelman,[6,*] and Bradford B. Lowell[1,*]

[1] Department of Medicine, Division of Endocrinology, Beth Israel Deaconess Medical Center and Harvard Medical School, Boston, Massachusetts 02215
[2] Clinic III for Internal Medicine, University of Cologne, 50937 Cologne, Germany
[3] Department of Internal Medicine
[4] Department of Cellular & Molecular Physiology
[5] Howard Hughes Medical Institute
Yale University School of Medicine, New Haven, Connecticut 06520
[6] Dana-Farber Cancer Institute and Department of Cell Biology, Harvard Medical School, Boston, Massachusetts 02115
[7] Institute of Normal Human Morphology, Faculty of Medicine, University of Marche, 60020 Ancona, Italy
[8] These authors contributed equally to this work.
[9] Present address: Department of Internal Medicine, Center for Hypothalamic Research, University of Texas Southwestern Medical Center, Dallas, Texas 75390.
*Correspondence: bruce_spiegelman@dfci.harvard.edu (B.M.S.), blowell@bidmc.harvard.edu (B.B.L.)

Summary

PGC-1β is a transcriptional coactivator that potently stimulates mitochondrial biogenesis and respiration of cells. Here, we have generated mice lacking exons 3 to 4 of the *Pgc-1*β gene (*Pgc-1*$\beta^{E3,4-/E3,4-}$ mice). These mice express a mutant protein that has reduced coactivation activity on a subset of transcription factors, including ERRα, a major target of PGC-1β in the induction of mitochondrial gene expression. The mutant mice have reduced expression of OXPHOS genes and mitochondrial dysfunction in liver and skeletal muscle as well as elevated liver triglycerides. Euglycemic-hyperinsulinemic clamp and insulin signaling studies show that PGC-1β mutant mice have normal skeletal muscle response to insulin but have hepatic insulin resistance. These results demonstrate that PGC-1β is required for normal expression of OXPHOS genes and mitochondrial function in liver and skeletal muscle. Importantly, these abnormalities do not cause insulin resistance in skeletal muscle but cause substantially reduced insulin action in the liver.

Introduction

Type 2 diabetes mellitus (DM2) is one of the most common metabolic disorders worldwide and is a major cause of blindness, renal failure, limb gangrene, and cardiovascular disease (Kahn, 1998; Zimmet et al., 2001). The primary cause of DM2 remains to be understood. It is clear, however, that insulin resistance is an early feature of DM2 (Shulman, 2000). Insulin resistance is consistently found in DM2 subjects and may be detected decades before the onset of DM2 (Lillioja et al., 1988, 1993; Warram et al., 1990). Moreover, in subjects with a family history of DM2, insulin resistance is the best predictor for the development of DM2 (Lillioja et al., 1993; Warram et al., 1990).

Insulin resistance is the failure of target tissues to respond properly to insulin. Liver and skeletal muscle are among the major sites of insulin action. Insulin reduces liver glucose production and stimulates glucose uptake into skeletal muscle. The development of insulin resistance in these tissues accounts for major alterations in glucose metabolism seen in DM2 subjects. Various factors have been implicated as being causally related to insulin resistance (Lazar, 2005; Lowell and Shulman, 2005); nevertheless, the underlying cellular mechanisms of insulin resistance in these tissues remain to be fully elucidated.

Recently, two independent gene expression profile studies identified a set of genes consistently downregulated in skeletal muscle of DM2 patients, oxidative phosphorylation (OXPHOS) genes (Mootha et al., 2003; Patti et al., 2003). Among them were several genes encoding subunits of complexes I to V of the respiratory chain, which were modestly (20%) but coordinately reduced. Moreover, the same set of genes were also found to be reduced in prediabetics with a family history of DM2 (Patti et al., 2003), demonstrating that reduction of OXPHOS gene expression is present very early during the development of the disease and may have a causal role in the onset of DM2. Consistent with the downregulation of OXPHOS gene expression, other studies have reported an impairment of mitochondrial oxidative phosphorylation function in skeletal muscle of diabetic and prediabetic subjects (Kelley et al., 2002; Petersen et al., 2003, 2004; Ritov et al., 2005). For instance, young, lean, insulin-resistant offspring of parents with DM2 were found to have a 30% reduction in rates of mitochondrial ATP synthesis in skeletal muscle assessed by ^{31}P NMR, which was associated with increases in intramyocellular lipid content (Petersen et al., 2004). Furthermore, healthy, lean, elderly subjects were found to have severe skeletal muscle insulin resistance, which was associated with increased intramyocellular and hepatic triglyceride content and reduced rates of mitochondrial oxidative

phosphorylation activity compared to younger activity- and body-weight-matched volunteers (Petersen et al., 2003). Finally, recent studies in muscle biopsy samples obtained from patients with DM2 have found a direct correlation between electron transport chain activity and mitochondrial area and the rate of insulin-stimulated glucose disposal (Kelley et al., 2002; Ritov et al., 2005). While all of these studies have implicated mitochondrial dysfunction in the pathogenesis of insulin resistance in humans, it remains to be determined whether mitochondrial dysfunction precedes or follows the development of insulin resistance.

Of note, peroxisome proliferator activator receptor γ coactivator 1α (PGC-1α) and 1β (PGC-1β) were also significantly less expressed in insulin-resistant skeletal muscle (Mootha et al., 2003; Patti et al., 2003). In contrast, Morino et al. (2005) have recently shown that PGC-1α and PGC-1β expression in skeletal muscle of young, lean, insulin-resistant offspring of parents with DM2 is not altered. PGC-1α is a transcriptional coactivator that has been shown to modulate the expression of many genes in different biological programs (Puigserver and Spiegelman, 2003) including mitochondrial oxidative metabolism in vitro and in vivo. It promotes mitochondrial biogenesis and cellular respiration in several cell types, and also does so when expressed transgenically in mice (Lehman et al., 2000; St-Pierre et al., 2003; Wu et al., 1999). Moreover, DNA microarray analysis following adenovirally mediated PGC-1α expression in C2C12 muscle cells has shown increased expression of a subset of OXPHOS genes that greatly overlap with those downregulated in skeletal muscle of diabetic/prediabetic humans (Mootha et al., 2004). Consistent with this, a large number of OXPHOS genes were shown to be reduced by 20%–50% in skeletal muscle of *Pgc-1α* null mice (Arany et al., 2005).

PGC-1β was recently identified as the closest homolog to PGC-1α (Lin et al., 2002a). PGC-1β has a wide tissue distribution, but it is most highly expressed in tissues of high oxidative metabolism such as brown adipose tissue (BAT), heart, and skeletal muscle (Lin et al., 2002a). It coactivates a broad range of nuclear receptors and transcription factors (Kressler et al., 2002; Lin et al., 2002a; Meirhaeghe et al., 2003) that partially overlap with PGC-1α's target transcription factors. There are also transcription factors that are exclusively coactivated by PGC-1β but not PGC-1α, such as the SREBP family (Lin et al., 2005). PGC-1β has been far less studied than PGC-1α; nevertheless, there is evidence that PGC-1β also regulates mitochondrial metabolism. Adenovirally mediated PGC-1β expression in muscle cells, primary rat hepatocytes, and rat liver induces the expression of genes of mitochondrial oxidative metabolism, such as cytochrome *c* and β-ATPase (Lin et al., 2003; St-Pierre et al., 2003). In addition, PGC-1β strongly promotes mitochondrial proliferation and cell respiration in muscle cells, (St-Pierre et al., 2003). These results strongly suggest that PGC-1β is a major regulator of mitochondrial metabolism.

In the present study, we have generated mice lacking exons 3 to 4 of the *Pgc-1β* gene (*Pgc-1β*$^{E3,4-/E3,4-}$ mice) and used these animals to investigate the function of PGC-1β in mitochondrial gene expression and function in liver and skeletal muscle. We have also directly addressed the question of whether a mutation in *Pgc-1β* causes insulin resistance in mice.

Results

Generation of PGC-1β mutant mice

Mice homozygous for the *Pgc-1β* allele lacking sequences from exon 3 to exon 4 (*Pgc-1β*$^{E3,4-/E3,4-}$) (Figure 1A) were generated. Our strategy was originally designed in an attempt to generate *Pgc-1β* null mice. The sequence from exons 3 to 4, containing two out of the three LXXLL motifs present in mouse PGC-1β, was replaced by a neomycin cassette such that the splicing acceptor sequences of exon 3 were retained and the splicing donor sequences of intron 4 were deleted. Our expectation was that the neomycin cassette would be retained in the mature mRNA and thus disrupt the reading frame of PGC-1β. However, this cassette was spliced out of the mature mRNA, and a mutant transcript lacking the sequence from exon 3 to exon 4 was generated. Heterozygous mice (*Pgc-1β*$^{+/E3,4-}$) were mated, and wild-type (WT), heterozygous, and homozygous offspring (Figure 1B) were obtained at the ratio consistent with Mendelian transmission (1:2:1), thus indicating that deletion of exons 3 to 4 of *Pgc-1β* does not cause lethality. The absence of transcripts containing exons 3 and 4 was verified by northern blot analyses. Total RNA samples from BAT and heart were analyzed with a probe spanning exons 3 to 4. Both PGC-1β transcripts (~9 and 4 kb) were detected in *Pgc-1β*$^{+/+}$ RNA samples but were absent in *Pgc-1β*$^{E3,4-/E3,4-}$ RNA samples (Figure 1C), indicating the absence of mRNA containing exons 3 and 4 in *Pgc-1β*$^{E3,4-/E3,4-}$ mice. In addition, total RNA of BAT was analyzed with a probe spanning exon 5 of *Pgc-1β*, which is outside of the deleted region. Again, two *Pgc-1β* transcripts were observed in the *Pgc-1β*$^{+/+}$ BAT RNA sample. However, two *Pgc-1β* transcripts were also observed in the *Pgc-1β*$^{E3,4-/E3,4-}$ BAT RNA sample. These were approximately 0.3 kb smaller than the former (Figure 1D). The combined length of exons 3 and 4 is 330 nucleotides, and a splicing event from exon 2 to exon 5 in *Pgc-1β* heterogeneous nuclear RNA was a possible explanation for the occurrence of such transcripts in *Pgc-1β*$^{E3,4-/E3,4-}$ mice. This possibility was tested by RT-PCR analysis of BAT, liver, and muscle total RNA using primers spanning exons 2 to 5. Amplicons of ~1.1 kb and ~0.8 kb were observed in *Pgc-1β*$^{+/+}$ and *Pgc-1β*$^{E3,4-/E3,4-}$ samples, respectively (Figure 1E). The splicing event from *Pgc-1β* exon 2 to exon 5 in *Pgc-1β*$^{E3,4-/E3,4-}$ mice was confirmed by sequencing of the latter (0.8 kb) amplicon. The nucleotide sequence of transcripts lacking exons 3 and 4 is in frame with *Pgc-1β*'s start codon, and the predicted amino acid sequence would lack 110 amino acids (from aa 85 to aa 194). The presence of this protein was confirmed in BAT lysates by western blot analyses using antisera raised against the N-terminal region of PGC-1β (aa 1 to aa 350) (Figure 1F). Of note, the amount of PGC-1β mutant (MT) protein detected was substantially reduced. However, this must be due to decreased antigen reactivity resulting from the lack of protein encoded by exons 3 and 4 since we have demonstrated that the PGC-1β antiserum detects the MT protein at an efficiency of ~25%–50% compared to the WT protein (Figure 1F; see also Figure S4 in the Supplemental Data available with this article online). Thus, expression of the mutant protein is approximately equal to expression of the WT protein.

Reduced coactivation of a subset of nuclear receptors by PGC-1β mutant protein

The LXXLL sequence is a very important ligand-dependent nuclear hormone receptor-interacting motif of nuclear receptors

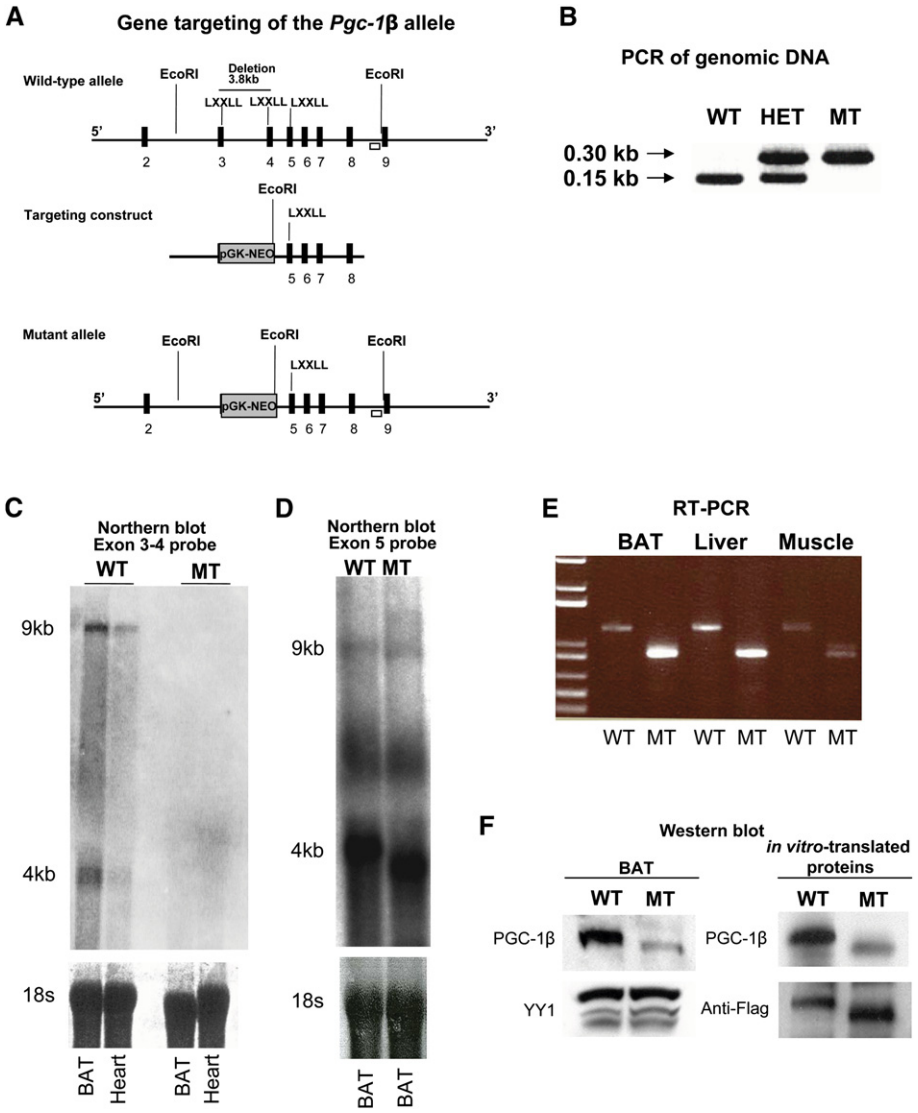

Figure 1. Generation of *Pgc-1*$\beta^{E3,4-/E3,4-}$ mice

A) Schematic representation of the wild-type *Pgc-1*β allele, the targeting construct, and the mutant *Pgc-1*β allele after homologous recombination. Exons are represented by filled boxes. EcoRI restriction sites and the probe (represented by an open box) used for Southern blot for genotyping of ES clones are shown. The deletion of exons 3 to 4 includes two out of the three canonical LXXLL motifs present in the wild-type *Pgc-1*β gene.

B) Genotyping by PCR analysis of tail genomic DNA of offspring of heterozygous (HET) crosses. The 150 bp and 300 bp amplicons for the wild-type (WT) and mutant (MT) *Pgc-1*β alleles, respectively, are indicated.

C) Northern blot analysis of brown fat (BAT) and heart total RNA. A probe spanning *Pgc-1*β exons 3 and 4 was used. *Pgc-1*β mRNA signal was detected as two bands at ~9 and ~4 kb in *Pgc-1*$\beta^{+/+}$ BAT and heart samples.

D) Northern blot analysis of BAT total RNA. A probe spanning *Pgc-1*β exon 5 was used. *Pgc-1*β mRNA was detected as two bands at ~9 and ~4 kb in the *Pgc-1*$\beta^{+/+}$ BAT mRNA sample. The MT *Pgc-1*β mRNA was detected as two bands at ~8.7 and ~3.7 kb in the *Pgc-1*$\beta^{E3,4-/E3,4-}$ BAT mRNA sample.

E) RT-PCR analysis of BAT, liver, and skeletal muscle total RNA using primers located in *Pgc-1*β exons 2 and 5. The amplicons were 650 bp and 350 bp for WT (left lanes) and MT (right lanes) mRNAs, respectively.

F) Western blot analysis using rabbit polyclonal antisera against the N terminus (aa 1–350) of the mouse PGC-1β as the primary antibody. (Left panel) The specific signal for PGC-1β was detected at ~160 kDa in *Pgc-1*$\beta^{+/+}$ BAT lysate. The PGC-1β MT signal was detected at ~150 kDa in *Pgc-1*$\beta^{E3,4-/E3,4-}$ BAT lysate. (Right panel) In vitro-translated WT or MT PGC-1β proteins were used as controls. To control for equal loading, rabbit polyclonal antisera against YY1 (left panel) and mouse monoclonal anti-FLAG antibody (right panel) were used. Note the reduced affinity of the antisera against PGC-1β MT.

(see, e.g., Savkur and Burris, 2004). The human PGC-1β contains two LXXLL motifs, and the LXXLL motif encoded by exon 4 has been shown to be crucial for interaction with ERα (Kressler et al., 2002). Thus, it seemed likely that the amino acids encoded by exons 3 and 4 of PGC-1β, which includes two of three LXXLL motifs present in mouse PGC-1β, would be required for its coactivation activity toward some nuclear receptors. To test this, we transiently cotransfected H2.35 hepatoma cells with plasmids encoding nuclear receptors or other transcription factors and equal amounts of plasmids encoding the PGC-1β WT or PGC-1β MT protein. ERRα has been shown to be a critical factor in the earliest stages of mitochondrial biogenesis induced by PGC-1β (Mootha, et al., 2004; Schreiber et al., 2004). As shown in Figure 2A, ERRα transactivates its own promoter, and PGC-1β increases its transcriptional activity by ~14-fold; PGC-1β MT is substantially reduced in this activity, increasing reporter gene expression by only ~3-fold. NRF1 is also a crucial factor in mitochondrial gene expression induced by the PGC-1s (Mootha, et al., 2004). NRF1 binds to NRF1 recognition sites, and PGC-1β WT activates its transcriptional activity by nearly 3-fold. In contrast, activation by PGC-1β MT is negligible. Similarly, HCF fused to a Gal4 DNA-binding domain binds to Gal4 DNA-binding motifs (UAS), and PGC-1β WT increases its transcriptional activity by ~20-fold, whereas PGC-1β MT increases it by only ~5-fold (Figures 2B and 2C). These results suggest that amino acids encoded by exons 3 and 4 are required for full coactivation of the transcription factors ERRα, NRF1, and HCF. In sharp contrast, the mutant protein has nearly normal activity on several other transcription factors. SREBP1c fused to a Gal4 DNA-binding domain binds to a Gal4 luciferase reporter plasmid, and the WT increases its transcriptional activity by more than 3-fold (Figure 2D). PGC-1β MT increases its transactivation activity more than 2-fold. Similar results were also obtained using SREBP1c on a fatty-acid synthase promoter luciferase reporter plasmid (Figure S1A). Coactivation of LXRα and PPARγ by PGC-1β WT or PGC-1β MT was also tested (data not shown) in the absence and presence of their respective ligands, T0901317 and rosiglitazone. PGC-1β WT and PGC-1β MT were found to similarly activate those nuclear receptors in the absence and presence of their ligands. These results suggest that coactivation of SREBP1c, LXRα, and PPARγ is not greatly affected by deletion of amino acids encoded by exons

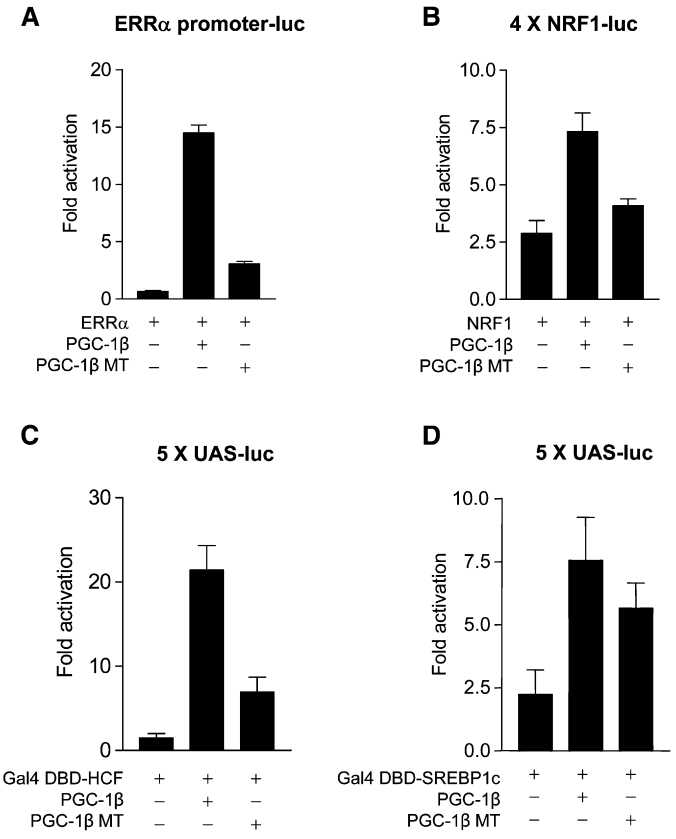

Figure 2. Reduced coactivation of a subset of nuclear receptors/transcription factors by PGC-1β mutant protein.

Mouse H2.35 hepatoma cells were transiently cotransfected with (**A**) ERRα-promoter luciferase reporter and ERRα plasmids, (**B**) 4× NRF1-luciferase reporter and NRF1 plasmids, (**C**) UAS-luciferase reporter and Gal-DBD-HCF plasmids, or (**D**) UAS-luciferase reporter and Gal-DBD-SREBP1c plasmids along with pCATCH-PGC-1β or pCATCH-PGC-1β mutant (MT) plasmids. pCMV-βGal was added for transfection efficiency normalization. Cells were harvested 48 hr after cotransfection and assayed for luciferase and β-galactosidase. The results represent the mean ± SEM of at least three independent experiments.

3 and 4. Taken together, these data suggest that amino acids 85 to 194 of PGC-1β are required for coactivation of ERRα, NRF1, and HCF, but likely not for coactivation of SREBP1c, LXRα, and PPARγ.

Reduced expression of OXPHOS genes in liver and skeletal muscle of PGC-1β mutant mice

To investigate whether this mutation in *Pgc-1β* results in alterations in gene expression and several physiological functions, we first performed transcriptional microarray analysis on RNA samples obtained from liver and skeletal muscle. In liver, clustering analysis of the microarray data revealed that expression of many genes of mitochondrial metabolism was downregulated by 30%–40% in *Pgc-1β*$^{E3,4-/E3,4-}$ mice compared to *Pgc-1β*$^{+/+}$ mice (Figure 3A). These genes include *Ndufv1*, *Ndufs1*, and *Ndufs7* (complex I subunits); *Uqcrc1* (complex III subunit); *Coq7* (ubiquinone synthesis); *Aco2* and *Dlst* (Krebs cycle); and *Sod2* (superoxide removal). *G6pc* and *Cyp7a* expression was also found to be reduced. To validate the reduced expression of these genes, we performed northern blot analysis (Figure 3B). Consistent with the microarray data, the northern blots confirmed a reduction in the expression of these genes. Importantly, all of the genes previously described as targets of PGC-1β-SREBP1c interaction (*Fasn*, *Scd1*, and *Hmgcr*) (Lin et al., 2005) were equally expressed in the livers of *Pgc-1β*$^{+/+}$ and *Pgc-1β*$^{E3,4-/E3,4-}$ mice. The LXRα target genes (*Pltp*, *Abca1*, *Abcg1*, *Abcg8*, and *Add1*) were similarly expressed in the two groups, with the exception of *Cyp7a*, which was markedly reduced in liver of *Pgc-1β*$^{E3,4-/E3,4-}$ mice. Quantitative PCR (qPCR) demonstrated that *Coq7* and *Ndufs1* mRNA levels were normal in heterozygous mice, suggesting no dominant-negative or gain-of-function effect of the mutant allele. *Ndufv1* mRNA levels were intermediate between wild-type and homozygous mice, which is consistent with a gene-dosage effect (Figure S1B). Finally, expression of *Pgc-1α* mRNA (as assessed by qPCR) was not altered in *Pgc-1β*$^{E3,4-/E3,4-}$ mice, indicating that PGC-1α did not compensate for decreased PGC-1β function in liver (data not shown).

Clustering analysis of the microarray data from quadriceps muscle revealed that expression of several genes of mitochondrial oxidative metabolism was reduced in *Pgc-1β*$^{E3,4-/E3,4-}$ RNA samples. These genes were reduced by 20%–30%, and most of them were OXPHOS genes encoding subunits of complexes I to V. Of note, *Ndufv1*, *Ndufa8*, *Ndufs1*, and *Ndufb10* (complex I subunits); *Sdhb* and *Sdhd* (complex II subunits); *Uqcr*, *Uqcrc1*, and *Uqcrc2* (complex III subunits); *Cox7a2* (complex IV subunit); *ATP5o* and *ATP5d* (complex V); and cytochrome *c* were all reduced in quadriceps muscle of *Pgc-1β*$^{E3,4-/E3,4-}$ mice (Figure 3C). qPCR assays were performed for selected OXPHOS genes to confirm the expression pattern shown by the microarray data. These studies revealed mRNA content to be reduced by ~30%–50% in quadriceps muscle of *Pgc-1β*$^{E3,4-/E3,4-}$ mice (Figure 3D). Quadriceps muscle is composed mostly of type II fibers (white, glycolytic), and we asked whether a similar reduction in those OXPHOS genes would be present in a muscle such as gastrocnemius, which contains both type I (red, oxidative) and type II fibers. The qPCR assays revealed a marked reduction (30%–60%) in mRNA content of OXPHOS genes in gastrocnemius of *Pgc-1β*$^{E3,4-/E3,4-}$ mice (Figure 3E). Also, we performed qPCR assays in gastrocnemius samples for genes encoding proteins characteristic of type I fibers, such as troponin I (slow) and myoglobin, which are under PGC-1α's regulation (Lin et al., 2002b). No differences in the expression of these genes were observed comparing samples of *Pgc-1β*$^{E3,4-/E3,4-}$ and *Pgc-1β*$^{+/+}$ mice (data not shown). Taken together, these results demonstrate conclusively that the amino acids encoded by exons 3 and 4 of PGC-1β are required for normal expression of many genes of mitochondrial oxidative metabolism in liver and skeletal muscle.

Reduced mitochondrial area and function in liver and skeletal muscle of PGC-1β mutant mice

PGC-1β has been shown to strongly stimulate mitochondrial biogenesis and cellular respiration in hepatocytes and muscle cells, suggesting that PGC-1β is a critical regulator of mitochondrial proliferation and function. To test this genetically, we first performed morphometric analysis of liver and skeletal muscle (extensor digitorum longus [EDL] and soleus) by quantitative electron microscopy. Liver and both types of skeletal muscle, EDL (white, glycolitic) and soleus (red, oxidative), of *Pgc-1β*$^{E3,4-/E3,4-}$ mice contained a number of mitochondria similar

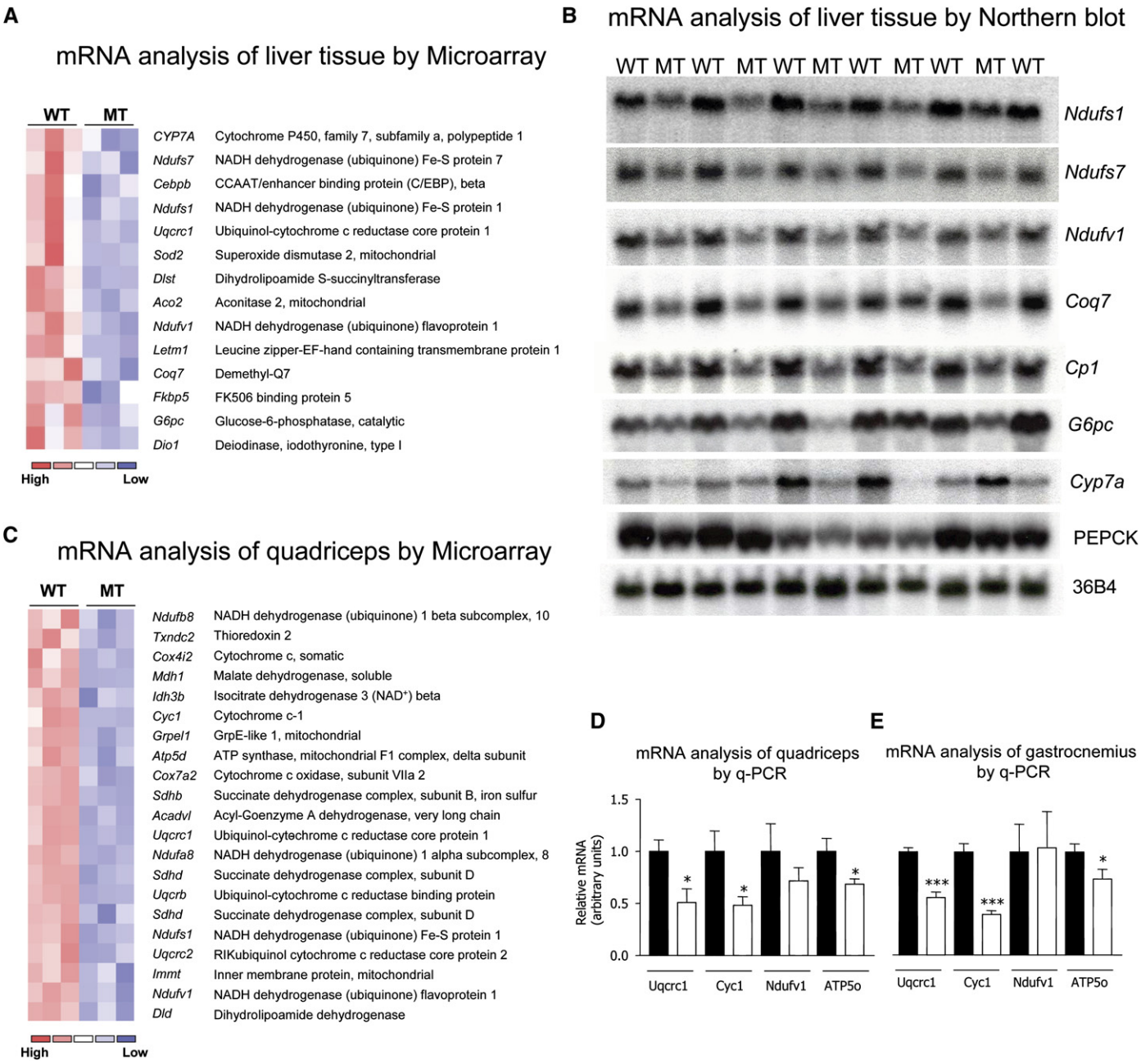

Figure 3. Reduced expression of OXPHOS genes in liver and skeletal muscle of *Pgc-1*$\beta^{E3,4-/E3,4-}$ mice

A) Clustering analysis of liver microarray data of *Pgc-1*$\beta^{+/+}$ (WT) and *Pgc-1*$\beta^{E3,4-/E3,4-}$ (MT) mRNA samples. Genes that were reduced in MT samples are indicated.

B) Northern blot analysis of WT and MT liver total RNA samples for validation of the microarray data. A probe specific for ribosomal protein 36B4 was included as a loading control.

C) Clustering analysis of quadriceps skeletal muscle microarray data from WT and MT mRNA samples. Genes reduced in MT samples are indicated.

D) TaqMan quantitative real-time PCR (qPCR) analysis of WT and MT quadriceps total RNA samples for validation of the microarray data. The mRNA content of specific genes was normalized to cyclophylin mRNA content. The mRNA levels are expressed relative to the WT values. Black bars represent WT; white bars represent MT. Results are expressed as mean ± SEM (n = 8–11). *p < 0.05; ***p < 0.001.

E) Expression of the same genes as in (**D**) was assessed by qPCR analysis of WT and MT gastrocnemius total RNA.

to that observed in samples derived from *Pgc-1*$\beta^{+/+}$ mice (Figures 4A–4C). However, mitochondrial area in liver, EDL, and soleus was greatly reduced in *Pgc-1*$\beta^{E3,4-/E3,4-}$ samples compared to *Pgc-1*$\beta^{+/+}$ samples (Figures 4D–4F).

We next assessed mitochondrial function as measured by O_2 consumption of isolated hepatocytes. A significant reduction of basal O_2 consumption (15%) was observed (Figure 4G). We also assessed complex IV (COX) activity, which is a critical component of the electron transport chain, in gastrocnemius muscle homogenates. COX activity of *Pgc-1*$\beta^{E3,4-/E3,4-}$ muscle homogenate was markedly reduced compared to that of *Pgc-1*$\beta^{+/+}$ mice (Figure 4H). These results show that PGC-1β is required to maintain normal mitochondrial function in liver and skeletal muscle.

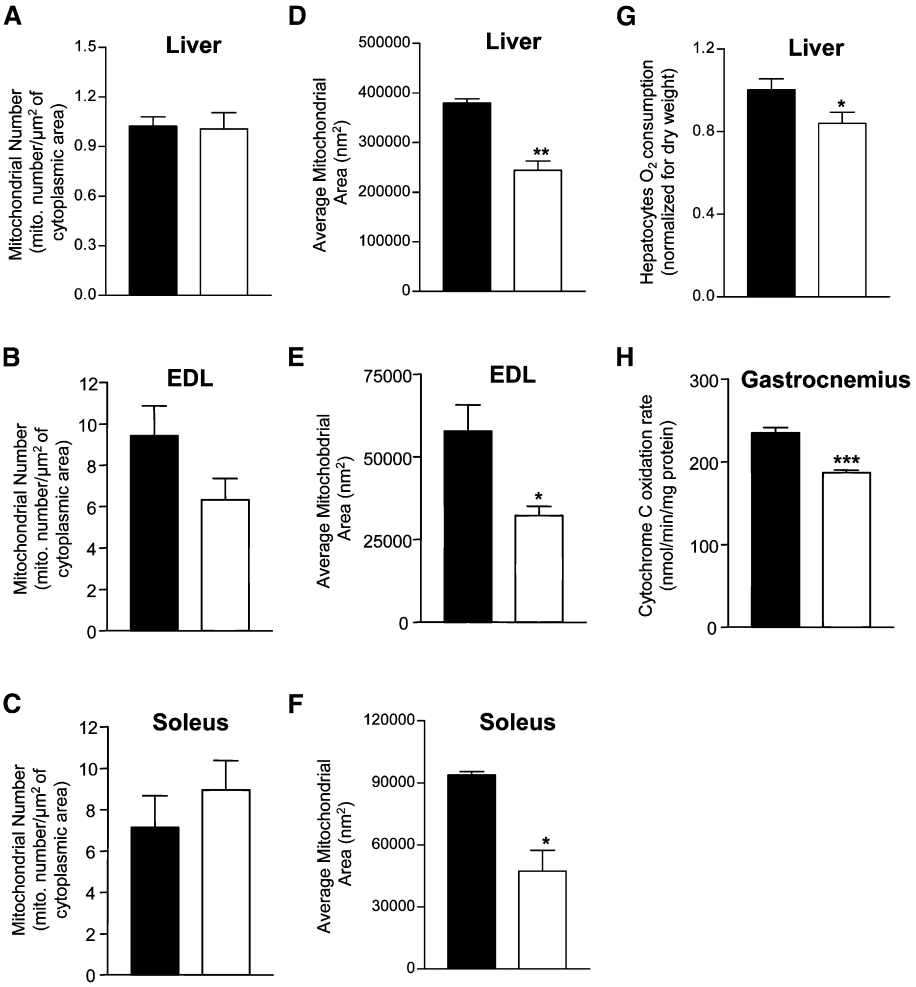

Figure 4. Reduced mitochondrial area and function in liver and skeletal muscle of *Pgc-1*$\beta^{E3,4-/E3,4-}$ mice

A–C) Mitochondria number on electron micrographs of liver (**A**), extensor digitorum longus (EDL; **B**), and soleus skeletal muscles (**C**) from *Pgc-1*$\beta^{+/+}$ and *Pgc-1*$\beta^{E3,4-/E3,4-}$ mice. Bars represent samples derived from *Pgc-1*$\beta^{+/+}$ (black) and *Pgc-1*$\beta^{E3,4-/E3,4-}$ mice (white). Results are expressed as mean ± SEM (n = 3–8). *p < 0.05; **p < 0.01; ***p < 0.001.

D–F) Average mitochondrial area was obtained by computer-assisted morphometry on electron micrographs of liver (**D**), EDL (**E**), and soleus skeletal muscles (**F**) from *Pgc-1*$\beta^{+/+}$ and *Pgc-1*$\beta^{E3,4-/E3,4-}$ mice.

G) Basal O_2 consumption was measured in hepatocytes of *Pgc-1*$\beta^{+/+}$ and *Pgc-1*$\beta^{E3,4-/E3,4-}$ mice.

H) Cytochrome *c* activity of gastrocnemius skeletal muscle samples of *Pgc-1*$\beta^{+/+}$ and *Pgc-1*$\beta^{E3,4-/E3,4-}$ mice.

Increased hepatic triglyceride content in the liver of PGC-1β mutant mice

Despite clear data indicating that this is an early correlate of insulin resistance in humans, it is unclear whether reduced expression of the PGC-1 coactivators and OXPHOS genes is a causal factor in insulin resistance. Thus, we investigated several parameters involved in insulin/glucose homeostasis in *Pgc-1*$\beta^{E3,4-/E3,4-}$ mice. As shown in Table 1, both genotypes had similar blood glucose and fatty-acid serum levels in both the fed and fasted states. Serum triglycerides levels tended to be lower in fed *Pgc-1*$\beta^{E3,4-/E3,4-}$ mice but similar in both genotypes in fasted mice (Table 1). Cholesterol and insulin serum levels were normal in fed *Pgc-1*$\beta^{E3,4-/E3,4-}$ mice. However, a trend toward elevated insulin serum levels was observed in fasted *Pgc-1*$\beta^{E3,4-/E3,4-}$ mice (Table 1). Body weight was not different between PGC-1β WT and MT mice (data not shown). Serum adiponectin levels, total body fat content, and subscapular brown fat-pad weights were normal in *Pgc-1*$\beta^{E3,4-/E3,4-}$ mice (Table 1). Impairment of mitochondrial oxidative metabolism may cause lipid accumulation, which has been strongly associated with insulin resistance in liver and skeletal muscle (Shulman, 2000). Thus, we measured triglyceride content in liver and skeletal muscle. Triglycerides were significantly increased in *Pgc-1*$\beta^{E3,4-/E3,4-}$ livers compared to *Pgc-1*$\beta^{+/+}$ livers, but not in quadriceps, gastrocnemius, or soleus muscles (Table 1). Of note, liver triglyceride levels were normal in heterozygous mice (Figure S1C).

Hepatic insulin resistance in PGC-1β mutant mice

To further investigate insulin sensitivity and whole-body glucose homeostasis, euglycemic-hyperinsulinemic clamp studies were performed (Figures 5A–5D). Glucose infusion rate during the clamps was similar in *Pgc-1*$\beta^{E3,4-/E3,4-}$ mice and *Pgc-1*$\beta^{+/+}$ mice (Figures 5A and 5B). Whole-body glycolysis and glycogen synthesis were also similar in both genotypes (Figure 5C). Skeletal muscle glucose uptake was also similar (Figure 5C), indicating the absence of skeletal muscle insulin resistance in *Pgc-1*$\beta^{E3,4-/E3,4-}$ mice. However, while insulin significantly reduced hepatic glucose production rates in *Pgc-1*$\beta^{+/+}$ mice during the euglycemic-hyperinsulinemic clamp, it had no effect on hepatic glucose production rates in *Pgc-1*$\beta^{E3,4-/E3,4-}$ mice (Figure 5D). These results indicate the presence of striking insulin resistance in the liver of the PGC-1β mutant mice.

To further explore the mechanism for this, we measured the ability of insulin to activate the PI3K-Akt pathway in liver and muscle of the PGC-1β mutant mice. Specifically, we assessed IRS-associated PI3-kinase activity and AKT activity in liver and muscle in response to the hyperinsulinemic conditions of the clamp (Figures 5E and 5F). Insulin-stimulated IRS-1-associated PI3-kinase activity and Akt activity were similar in WT and

Table 1. Body and blood composition of *Pgc-1*$\beta^{+/+}$ (WT) and *Pgc-1*$\beta^{E3,4-/E3,4-}$ (MT) male mice

	WT	MT
Glucose (mg/dl)		
Fed	129 ± 7 (10)	127 ± 6 (11)
Fasted	63 ± 3 (13)	66 ± 2 (13)
Insulin (ng/ml)		
Fed	1.41 ± 0.13 (14)	1.62 ± 0.13 (15)
Fasted	0.28 ± 0.07 (13)	0.36 ± 0.05 (16)
Adiponectin (μg/ml)		
Fed	8.69 ± 0.99 (6)	8.98 ± 1.04 (6)
Fatty acids (mM)		
Fed	0.67 ± 0.05 (11)	0.77 ± 0.07 (10)
Fasted	1.38 ± 0.09 (14)	1.28 ± 0.09 (13)
Triglycerides (mg/dl)		
Fed	90.3 ± 12.7 (9)	64.8 ± 8.0 (9)
Fasted	109.8 ± 23.2 (6)	84.7 ± 24.9 (6)
Cholesterol (mg/dl)		
Fed	148.2 ± 11.3 (5)	158.8 ± 12.5 (5)
Liver triglycerides (mg/g tissue)		
Fed	3.82 ± 0.58 (13)	7.76 ± 0.75 (14)*
Muscle triglycerides (mg/g tissue)		
Quadriceps	6.61 ± 2.54 (4)	2.39 ± 1.21 (4)
Gastrocnemius	4.11 ± 0.81 (10)	3.81 ± 1.28 (8)
Soleus	10.07 ± 2.31 (6)	11.86 ± 2.45 (6)
White adipose tissue (WAT) mass		
Tissue mass (g)	4.85 ± 0.88 (5)	4.99 ± 0.59 (5)
Ratio of WAT mass to body mass (%/g)	20.58 ± 2.35 (5)	21.76 ± 2.94 (5)
Brown adipose tissue fat-pad weight (mg)		
Subscapular	87.9 ± 15.29 (8)	83.5 ± 14.60 (6)

Parameters were assessed in mice at 9–12 weeks of age. All data represent mean ± SEM. The number of animals per group is shown in parentheses.
* $p < 0.05$.

mutant gastrocnemius samples. In liver of *Pgc-1*$\beta^{E3,4-/E3,4-}$ mice, insulin-stimulated IRS-2-associated PI3-kinase activity tended to be reduced, and Akt activity was significantly reduced compared to WT samples. These results demonstrate reduction of biochemical actions of insulin in liver of *Pgc-1*$\beta^{E3,4-/E3,4-}$ mice, but no alterations in skeletal muscle. Together, these results suggest that insulin resistance in the liver of *Pgc-1*$\beta^{E3,4-/E3,4-}$ mice is explained, at least in part, by decreased insulin-stimulated PI3K-Akt activation.

Finally, to assess whether this liver insulin resistance would cause whole-body glucose intolerance and/or insulin resistance, intraperitoneal insulin tolerance tests (ITTs) and glucose tolerance tests (GTTs) were performed on mice of both genotypes. At both 4 and 9 months of age, *Pgc-1*$\beta^{+/+}$ and *Pgc-1*$\beta^{E3,4-/E3,4-}$ mice had similar blood glucose concentrations during GTTs (data not shown). Also, according to the ITTs in 4- and 9-month-old mice, a similar suppression of blood glucose levels was observed in both *Pgc-1*$\beta^{+/+}$ and *Pgc-1*$\beta^{E3,4-/E3,4-}$ mice (Figures 6A and 6B). These results indicate that although *Pgc-1*$\beta^{E3,4-/E3,4-}$ mice have quite significant hepatic insulin resistance, there is sufficient compensation by other tissues and/or physiological systems to prevent whole-body glucose intolerance and/or insulin resistance. Finally, to see whether *Pgc-1*$\beta^{E3,4-/E3,4-}$ mice have altered sensitivity to high-fat-diet-induced insulin resistance, we fed mice a high-fat diet for 12 weeks. Glucose levels in the fed state were equal in wild-type and *Pgc-1*$\beta^{E3,4-/E3,4-}$ mice (data not shown). Also, insulin tolerance tests were similar in high-fat-fed wild-type versus *Pgc-1*$\beta^{E3,4-/E3,4-}$ mice (Figure S2A).

Discussion

Several reports have suggested that reduced expression of genes encoding mitochondrial enzymes of oxidative phosphorylation (OXPHOS) in skeletal muscle could play a critical role in causing insulin resistance. However, whether these alterations precede and cause the development of insulin resistance is presently unknown (Lowell and Shulman, 2005). In this report, we were able to address this question in mice. To study the function of the transcriptional coactivator PGC-1β, which has been suggested to regulate the expression of genes of mitochondrial oxidative metabolism, we have generated mice lacking exons 3 to 4 of the *Pgc-1*β gene (*Pgc-1*$\beta^{E3,4-/E3,4-}$ mice). These mice have reduced expression of several OXPHOS genes as well as smaller and functionally impaired mitochondria in liver and skeletal muscle. The data presented here show conclusively an important role for PGC-1β as a regulator of mitochondrial biology in vivo. Furthermore, the *Pgc-1*$\beta^{E3,4-/E3,4-}$ mice were used as a model to test whether a mutation in *Pgc-1*β and subsequent mitochondrial dysfunction causes insulin resistance. Importantly, *Pgc-1*$\beta^{E3,4-/E3,4-}$ mice are not hyperactive (Figure S2A) and have body weight (data not shown) and fat mass (Table 1) similar to *Pgc-1*$\beta^{+/+}$ littermates, making it feasible to assess whether a primary reduction of OXPHOS genes is sufficient to cause insulin resistance in muscle or liver. Similar rates of skeletal muscle glucose uptake in response to insulin were observed in both genotypes of mice, indicating similar degrees of skeletal muscle insulin sensitivity in *Pgc-1*$\beta^{E3,4-/E3,4-}$ and *Pgc-1*$\beta^{+/+}$ mice. Furthermore, insulin signaling in skeletal muscle, as assessed by Akt and IRS-1-associated PI3-kinase activity, was similar in *Pgc-1*$\beta^{E3,4-/E3,4-}$ and *Pgc-1*$\beta^{+/+}$ mice. Finally, a similar suppression of blood glucose levels was also observed in ITTs of both *Pgc-1*$\beta^{+/+}$ and *Pgc-1*$\beta^{E3,4-/E3,4-}$ mice fed a high-fat diet (Figure S2B). These results suggest that PGC-1β-mediated reductions in expression of OXPHOS genes per se do not cause insulin resistance in skeletal muscle.

It is possible, however, that downregulation of OXPHOS genes leads to the development of skeletal muscle insulin resistance, but only in the presence of other mitochondrial alterations that are absent in *Pgc-1*$\beta^{E3,4-/E3,4-}$ mice. Despite the fact that skeletal muscle mitochondria were functionally abnormal, we did not observe any associated increases in intracellular lipid content, which would have been anticipated if mitochondrial fatty-acid oxidation was also impaired. Intramyocellular triglyceride accumulation—and more importantly, increases in intracellular diacylglycerol content—has been shown to cause insulin resistance in skeletal muscle, and it is likely that its presence is required for the development of insulin resistance (Dresner et al., 1999; Griffin et al., 1999; Yu et al., 2002). On the other hand, it is also plausible that reduced expression of PGC-1α or PGC-1β is causally implicated in skeletal muscle insulin resistance, but independently of the expression of OXPHOS genes. Indeed, PGC-1α has been shown to regulate the expression of Glut4 in muscle cells (Michael et al., 2001) and has also been shown to control the formation of type I fibers (Lin, et al., 2002b), the most insulin-sensitive type of skeletal muscle fiber. Further studies with specific deletion of PGC-1α and PGC-1β in skeletal muscle are required to definitively address these questions.

In contrast, this mutation in *Pgc-1*β clearly causes dysfunction in the liver, including the induction of insulin resistance. PGC-1β

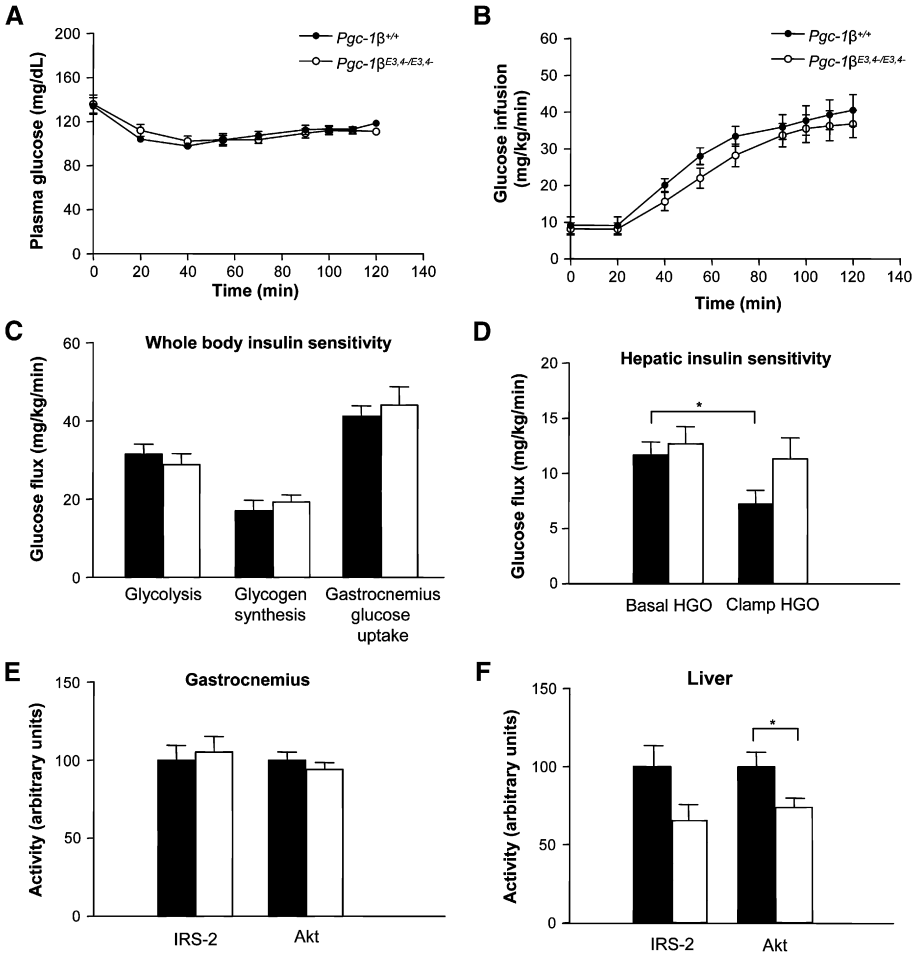

Figure 5. Euglycemic-hyperinsulinemic clamp study and intracellular insulin signaling in *Pgc-1*$\beta^{E3,4-/E3,4-}$ mice

Mice were injected with 2.5 mU/kg/min of insulin. Bars and circles represent *Pgc-1*$\beta^{+/+}$ (black) and *Pgc-1*$\beta^{E3,4-/E3,4-}$ (white) mice. Results are expressed as mean ± SEM (n = 6–11). *$p < 0.05$.

A–D) Euglycemic-hyperinsulinemic clamp studies were performed on chow-fed 18- to 20-week-old *Pgc-1*$\beta^{+/+}$ and *Pgc-1*$\beta^{E3,4-/E3,4-}$ male mice.

A and B) Plasma glucose levels (**A**) and glucose infusion rate during clamp study (**B**) are shown.

C and D) Whole-body glycolysis, glycogen synthesis, and gastrocnemius glucose uptake (**C**) and hepatic insulin sensitivity parameters (**D**) are shown.

E and F) IRS-1- or IRS-2-associated PI3-kinase activity and Akt activity in gastrocnemius (**E**) and liver (**F**) are shown.

has been recently shown to regulate the expression of lipogenic genes and genes involved in lipid secretion by liver via the coactivation of SREBP1c and likely LXRα, respectively (Lin et al., 2005). We show here that PGC-1β is also required in liver for normal expression of genes encoding mitochondrial proteins, including OXPHOS genes. However, according to the liver transcriptional profile data, PGC-1β-SREBP1c target genes were not reduced in *Pgc-1*$\beta^{E3,4-/E3,4-}$ mice. This may be explained by the fact that PGC-1β MT coactivates SREBP1c normally in vitro. Indeed, these data are consistent with the known SREBP1c docking site, which is located between amino acids 350 and 530 of PGC-1β, downstream of the region deleted in the mutant PGC-1β (aa 85 to aa 194) (Lin et al., 2005).

The *Pgc-1*$\beta^{E3,4-/E3,4-}$ mice also show reduced mitochondrial substrate oxidation, as assessed by oxygen consumption of isolated hepatocytes, as well as an accumulation of triglycerides in the liver. Since this hypomorphic mutation causes a deficiency in expression of mitochondrial genes and mitochondrial function, it seems very likely that this is largely a consequence of the poor coactivation of ERRα and NFR-1 by the mutant PGC-1β. However, loss of coactivation of other transcription factors as a contributing factor to the phenotype of these mice also seems likely.

To examine the possibility that the *Pgc-1*$\beta^{E3,4-/E3,4-}$ mutant allele could be functioning as a dominant-negative and/or gain-of-function mutant or, alternatively, as a simple

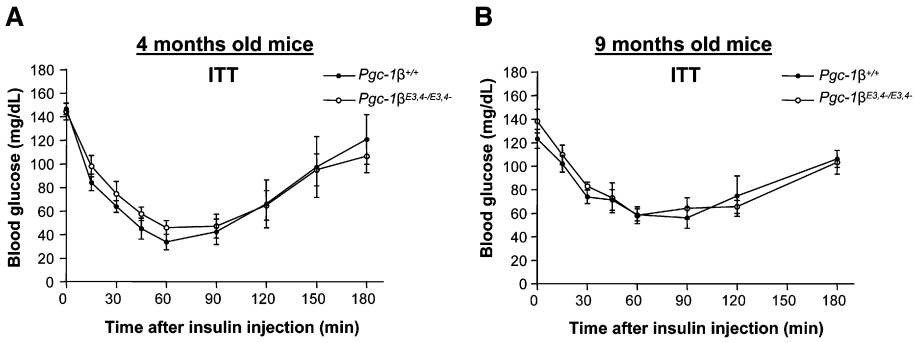

Figure 6. Insulin tolerance tests in aged *Pgc-1*$\beta^{+/+}$ and *Pgc-1*$\beta^{E3,4-/E3,4-}$ male mice

Intraperitoneal insulin tolerance tests (ITT) were performed in 4-month-old (**A**) and 9-month-old (**B**) *Pgc-1*$\beta^{+/+}$ and *Pgc-1*$\beta^{E3,4-/E3,4-}$ male mice. Following 4 hr without food, mice were injected with insulin at 1.5 U/kg of body weight. Results are expressed as mean ± SEM (n = 5–8).

loss-of-function mutant, we studied heterozygous animals. If the mutant functioned in a dominant-negative and/or gain-of-function manner, heterozygotes would be predicted to have abnormalities similar to those observed in homozygotes. We assessed *Coq7*, *Ndufv1*, and *Ndufs1* mRNA expression in liver as well as triglyceride levels in liver, four parameters that were markedly abnormal in homozygous mice. Of note, in heterozygous mice, *Coq7* and *Ndufs1* mRNA levels, as well as triglyceride levels, were unchanged compared to wild-type mice. *Ndufv1* mRNA levels were intermediate between wild-type and homozygous mice which is consistent with a gene-dosage effect. Overall, these findings strongly suggest that abnormalities observed in *Pgc-1*$\beta^{E3,4-/E3,4-}$ mice are due to loss of PGC-1β function and are not due to dominant-negative and/or gain-of-function effects.

An association between intrahepatic lipid accumulation and insulin resistance was observed in several previous studies of other animal models (Kim et al., 2000; Neschen et al., 2005; Samuel et al., 2004). Of course, other explanations for the intrahepatic lipid accumulation include increased hepatic lipogenesis or reduced lipoprotein secretion. Consistent with the possibility of reduced lipoprotein secretion, serum TG levels tended to be reduced in *Pgc-1*$\beta^{E3,4-/E3,4-}$ mice. Related to this, it was recently shown that PGC-1β coactivates Foxa2 and induces expression of microsomal transfer protein (MTP), facilitating the secretion of VLDLs (Wolfrum and Stoffel, 2006). Given this, it is possible that MTP expression could be decreased in *Pgc-1*$\beta^{E3,4-/E3,4-}$ mice and, as such, could contribute to hepatic steatosis. This scenario, however, is unlikely since *Mtp* mRNA expression was not altered in *Pgc-1*$\beta^{E3,4-/E3,4-}$ mice (Figure S1D).

In summary, these results demonstrate that PGC-1β is required for normal expression of OXPHOS genes and mitochondrial function in the liver and suggest that mitochondrial dysfunction may be a cause of hepatic insulin resistance. An understanding of the full range of the physiological effects of deletion of PGC-1β must await creation of mice carrying a null mutation.

Experimental procedures

Generation of PGC-1β mutant mice

The targeting plasmid was constructed using a BAC clone containing genomic DNA derived from the SV129 mouse strain. Replacement of the *Pgc-1*β gene exons 3 to 4 by a neomycin cassette, as well as cloning of DNA in pGEM-T Easy Vector (Promega) for transfection of ES cells, was performed using homologous recombination in the EL250 bacteria strain as described by Lee et al. (2001). ES cell electroporation, selection, and screening were performed using standard techniques. Neomycin-resistant ES cell clones were screened for 5′ and 3′ end recombination. Screening of 3′ end recombination was performed by Southern blot (Figure S3A). The DNA of ES cell clones was digested with EcoRI and analyzed with a probe outside of the construct. Screening for 5′ end recombination was performed by PCR (Figure S3B). The ES clones with recombination of both ends (5′ and 3′ end) were injected into blastulas. The chimeric founders were bred to wild-type C57BL/6 mice, and heterozygous mice were bred to obtain mice homozygous for the wild-type *Pgc-1*β allele (*Pgc-1*$\beta^{+/+}$) and the mutant *Pgc-1*β allele (*Pgc-1*$\beta^{E3,4-/E3,4-}$).

Animal care

All the experiments were performed in accordance with Beth Israel Deaconess Medical Center and Yale University Institutional Animal Care and Use Committee (IACUC) guidelines. Mice were housed in groups of two to four at 22°C–24°C in a 14 hr light/10 hr dark cycle and fed chow diet (Teklad F6 Rodent Diet 8664, Harlan Teklad) and water ad libitum. Mice were fed a high-fat, high-sucrose diet (Research Diets, D-12331) for 12 weeks where indicated. All studies were performed with male mice 9–12 weeks of age unless otherwise specified.

Transient transfections

pCATCH-*FLAG-Pgc-1*β was cloned as previously described (Lin et al., 2002a). To clone pCATCH-*FLAG-Pgc-1*β mutant, the region spanning exon 1 to exon 5 was first amplified by RT-PCR using BAT mRNA and the primers 5′-CCTGGATCCGCGGGGAACGACTGCGGCGC-3′ (sense) and 5′-GCCTTTGTTTCCGTTGGCAGAG-3′ (antisense) (non-*Pgc-1*β-specific sequence is underlined for the sense primer, which includes a BamHI site). The amplified product was digested with BamHI and cloned into BamHI sites of pCATCH-*FLAG-Pgc-1*β. pCATCH-*FLAG-Pgc-1*β mutant clone (MT) was verified by DNA sequencing.

H2.35 hepatoma cells (ATCC) were maintained in DMEM containing 4.5 g/l glucose and supplemented with 200 nM dexamethasone and 4% FBS. Transient transfections were performed using SuperFect Reagent (Promega) according to the manufacturer's instructions. Cells were transiently cotransfected with the indicated luciferase reporter (100 ng) and transcriptional factor/nuclear receptor (10–20 ng) plasmids and equal amounts of PGC-1β WT or PGC-1β MT plasmids (250–800 ng). pCMV-βGal (50 ng) was also included as a control for transfection efficiency normalization. pCATCH without inserted *Pgc-1*β was added if necessary for transfection of equal amounts of DNA. Cells were harvested after 48 hr of transfection for luciferase and β-galactosidase assays (Tropix Inc.).

Gene transcription profile

Total RNA was extracted from liver and skeletal muscle using the RNeasy Kit (QIAGEN), according to the manufacturer's instructions. Synthesis of cRNA, hybridization, and scanning of the Affymetrix Murine 430 2.0 chip was performed by the Dana-Farber Cancer Institute Microarray Core Facility. The microarray data were analyzed by clustering analysis using d-Chip software (Li and Wong, 2001). Microarray data were validated by northern blot or qPCR. For northern blots, 20 μg of total RNA per sample was separated on a formaldehyde gel, transferred to nylon membrane, and hybridized with gene-specific probes. For qPCR, cDNA was synthesized using the SuperScript First-Strand Synthesis System for RT-PCR (Invitrogen Corp.), and the amplifications were performed using TaqMan gene expression assays (Applied Biosystems). *Mtp* primer (forward: 5′-ATGATCCTCTTGGCAGTGCTT-3′; reverse: 5′-TGAGAGGCCAGTTGTGTGAC-3′) and probe (5′-TCTCTGCTTCTTCTCCTCCTACTCTGCTTC-3′) were synthesized by Biosearch Technologies, Inc.

Electromicrograph morphometry

Tissues were dissected and fixed in 4% paraformaldehyde in 0.1 M phosphate buffer (pH 7.4). Samples were subsequently dehydrated and embedded in plastic (JB-4, Electron Microscopy Sciences). Thin sections were obtained with an MTX ultramicrotome (RMC) and examined with a transmission electron microscope (CM10, Philips). Ten sections per sample were analyzed. Mitochondrial number represents the average of a total number of ~500 mitochondria analyzed per genotype.

O_2 consumption and complex IV activity

To isolate hepatocytes, mice were anesthetized, and liver was perfused for 3 and 4 min with prewarmed (42°C) liver perfusion and liver digestion media (Invitrogen), respectively. After perfusion, liver was quickly removed, minced, and put into DMEM supplemented with 20% FBS. The cell suspension was gently put through a cell strainer (70 μM) and collected in a Falcon tube. The media volume was brought to 40 ml, and the cells were pelleted. The pellets were resuspended in 30 ml of media. Cells were washed in media three times in total. At the end, the cells were resuspended in a small volume of DMEM for O_2 consumption assay. O_2 consumption was corrected by dry weight of cells. Complex IV activity was performed as previously described (Rustin et al., 1994). Gastrocnemius muscle samples were homogenized in PBS buffer (pH 7.0) (1:10 w/v) using a Teflon homogenizer. The homogenates were centrifuged (800 × g, 10 min) and the supernatants were diluted in SETH buffer (250 mM sucrose, 2 mM EDTA, 10 mM Tris-HCl, 50 U/ml heparin) at pH 7.4 for determination of cytochrome *c* oxidase activity. Activity was normalized by protein content.

Body composition analysis

Body composition was assessed by dual-energy X-ray absorptiometry (MEC LunarCorp). BAT mass was assessed by harvesting and weighing subscapular BAT fat pads.

Serum metabolites

Tail-vein blood was collected from fed or 24-hr-fasted 9- to 12-week-old mice. Blood was assayed for glucose level using a OneTouch FastTake glucometer (LifeScan Inc.), and serum was collected after blood centrifugation. Insulin levels were determined by Rat Insulin ELISA (Crystal Chem Inc.). Serum adiponectin levels were measured by Mouse Adiponectin ELISA (Linco Research). Serum fatty acids, triglycerides, and cholesterol were assayed using NEFA C, L-Type TG H, and Cholesterol CII kits, respectively (Wako Chemicals USA, Inc.).

Tissue triglycerides

To measure triglyceride content in liver and skeletal muscle, triglycerides were extracted using chloroform/MeOH. Approximately 100 mg of liver, quadriceps, and gastrocnemius muscle biopsies and ~9 mg of soleus muscle were homogenized for 1 min in 500 μl of buffer containing 50 mM Tris-HCl (pH 7.5), 5 mM EDTA, 300 mM mannitol, and 1 mM PMSF. Samples were kept on ice. Two hundred microliters of this mix was transferred into a new tube, and 5 μl of KOH and 800 μl of chloroform/MeOH (2:1) were added. Samples were vortexed vigorously, left for 5 min at room temperature, and centrifuged at 10,000 × g for 10 min. Five hundred microliters of the bottom layer was taken and mixed to an equal volume of chloroform/MeOH/H_2O (3:48:47). Samples were vortexed vigorously and spun at 10,000 × g for 10 min. One hundred and eighty microliters of the bottom layer was transferred to a new tube and dried completely overnight. Fifty microliters of butanol/[Triton-X114:MeOH (2:1)] (30:20) was added to the dried samples, and TG levels were assayed using the L-Type TG H Kit (Wako Chemicals USA, Inc.).

Euglycemic-hyperinsulinemic clamp studies and insulin tolerance tests

Euglycemic-hyperinsulinemic clamp studies were performed with *Pgc-1*$\beta^{+/+}$ and *Pgc-1*$\beta^{E3,4-/E3,4-}$ littermates of 18–20 weeks of age. Body fat and lean body mass were assessed by ^{1}H magnetic resonance spectroscopy (Bruker BioSpin). Six days before the experiment, an indwelling catheter was implanted into the left jugular vein. After an overnight fast, [3-^{3}H]glucose (HPLC-purified; PerkinElmer) was infused at a rate of 0.05 mCi/min for 2 hr to assess the basal glucose turnover. Following this period, euglycemic-hyperinsulinemic clamp study was conducted for 120 min with a primed and continuous infusion of human insulin (105 pmol/kg primed, 15 pmol/kg/min infusion) (Novo Nordisk), and 20% dextrose was infused at variable rates to maintain plasma glucose at basal concentrations (~6.7 mM). To estimate insulin-stimulated whole-body glucose fluxes, [3-^{3}H]glucose was infused at a rate of 0.1 mCi/min throughout the clamps, and 2-deoxy-D-[1-^{14}C]glucose (2-[^{14}C]DG; PerkinElmer) was injected as a bolus 75 min after the beginning of the clamp studies to estimate the rate of insulin-stimulated tissue glucose uptake. After the clamp studies, liver and gastrocnemius muscle were rapidly removed and stored for later analysis of insulin signaling. Whole-body and tissue glucose uptakes were calculated as previously described (Youn and Buchanan, 1993). For insulin tolerance tests, mice were fasted for 4 hr before receiving an intraperitoneal injection of insulin at 1.5 mU/g. Blood glucose levels were collected from tail before and at 15, 30, 60, 90, and 120 min after insulin infusion. Glucose levels were determined using a OneTouch FastTake glucometer (LifeScan Inc.).

Immunoblotting

BAT was homogenized in lysis buffer (50 mM Tris [pH 7.8], 137 mM NaCl, 10 mM NaF, 1 mM EDTA, 1% Triton X-100, 0.2% sarkosyl, 10% glycerol, and protease inhibitor), solubilized by continuous stirring for 1 hr at 4°C, and clarified by centrifugation. In vitro-translated proteins were prepared from 1 μg of wild-type and mutant pCATCH-*FLAG-Pgc-1*β plasmid DNA using the TnT T7 Coupled Reticulocyte Lysate System (Promega) according to the manufacturer's protocol. Tissue lysates and in vitro-translated proteins were separated by SDS-PAGE and transferred onto a nitrocellulose membrane by electroblotting. PGC-1β was detected using rabbit polyclonal antisera against the N terminus (aa 1–350) of the mouse PGC-1β. The in vitro-translated FLAG protein was detected using monoclonal ANTI-FLAG M2 antibody (Sigma).

Determination of IRS-1- or IRS-2-associated PI3K and Akt activity

To prepare gastrocnemius and liver lysates, 50 mg of tissue was homogenized using a polytron at half maximum speed for 1 min on ice in 500 μl buffer (20 mM Tris [pH 7.5], 5 mM EDTA, 10 mM $Na_4P_2O_7$, 100 mM NaF, 2 mM Na_3VO_4) containing 1% NP-40, 1 mM PMSF, 10 μg/ml aprotinin, and 10 μg/ml leupeptin. Tissue lysates were solubilized by continuous stirring for 1 hr at 4°C and centrifuged for 10 min at 14,000 × g. The supernatants were stored at −80°C until analysis. Tissue lysates (500 μg protein) were subjected to immunoprecipitation for 4 hr at 4°C with 5 μl of either a polyclonal IRS-1 antibody or a polyclonal IRS-2 antibody (1:100 dilution; gift from Dr. Morris White, Joslin Diabetes Center) or 2 μg of Akt antibody that recognizes both Akt1 and Akt2 (Upstate Biotechnology) coupled to protein A-Sepharose (Sigma) or protein G-Sepharose beads. The immune complex was washed, and PI3K and Akt activity were determined as described previously (Kim et al., 2002).

Statistical analysis

All results are expressed as means ± SEM. Two-tailed Student's t test was used to determine p values.

Supplemental data

Supplemental Data include four figures and can be found with this article online at http://www.cellmetabolism.org/cgi/content/full/4/6/453/DC1/.

Acknowledgments

We thank Dr. Chen-Yu Zhang for helpful discussions and Jia Yu for technical assistance with ES cell manipulation. We also thank Cleide G. da Silva and Marcelo A. Christoffolete for technical advice. This work was supported by grants DK61562 (B.M.S.) and DK49569 (B.B.L.) from the National Institutes of Health, grant 7-05-PPG-02 (Y.-B.K.) from the American Diabetes Association, grant KF-Nr. 31/2006 (M.H.) from the Köln Fortune Nachwuchsförderprogramm, and grant HU1583/1-1 (M.H.) from the Deutsche Forschungsgemeinschaft.

Received: February 9, 2006
Revised: October 3, 2006
Accepted: November 6, 2006
Published: December 5, 2006

References

Arany, Z., He, H., Lin, J., Hoyer, K., Handschin, C., Toka, O., Ahmad, F., Matsui, T., Chin, S., Wu, P.H., et al. (2005). Transcriptional coactivator PGC-1α controls energy state and contractile function of cardiac muscle. Cell Metab. *1*, 259–271.

Dresner, A., Laurent, D., Marcucci, M., Griffin, M.E., Dufour, S., Cline, G.W., Slezak, L.A., Andersen, D.K., Hundal, R.S., Rothman, D.L., et al. (1999). Effects of free fatty acids on glucose transport and IRS-1-associated phosphatidylinositol 3-kinase activity. Diabetes *103*, 253–259.

Griffin, M.E., Marcucci, M.J., Cline, G.W., Bell, K., Barucci, N., Lee, D., Goodyear, L.J., Kraegen, E.W., White, M.F., and Shulman, G.I. (1999). Free fatty acid-induced insulin resistance is associated with activation of protein kinase C theta and alterations in the insulin signaling cascade. Diabetes *48*, 1270–1274.

Kahn, B.B. (1998). Type 2 diabetes: When insulin secretion fails to compensate for insulin resistance. Cell *92*, 593–596.

Kelley, D.E., He, J., Menshikova, E.V., and Ritov, V.B. (2002). Dysfunction of mitochondria in human skeletal muscle in type 2 diabetes. Diabetes *51*, 2944–2950.

Kim, J.K., Gavrilova, O., Chen, Y., Reitman, M.L., and Shulman, G.I. (2000). Mechanism of insulin resistance in A-ZIP/F-1 fatless mice. J. Biol. Chem. *275*, 8456–8460.

Kim, Y.B., Shulman, G.I., and Kahn, B.B. (2002). Fatty acid infusion selectively impairs insulin action on Akt1 and protein kinase C lambda/zeta but not on glycogen synthase kinase-3. J. Biol. Chem. *277*, 32915–32922.

Kressler, D., Schreiber, S.N., Knutti, D., and Kralli, A. (2002). The PGC-1-related protein PERC is a selective coactivator of estrogen receptor alpha. J. Biol. Chem. *277*, 13918–13925.

Lazar, M.A. (2005). How obesity causes diabetes: Not a tall tale. Science *307*, 373–375.

Lee, E.C., Yu, D., Martinez de Velasco, J., Tessarollo, L., Swing, D.A., Court, D.L., Jenkins, N.A., and Copeland, N.G. (2001). A highly efficient Escherichia coli-based chromosome engineering system adapted for recombinogenic targeting and subcloning of BAC DNA. Genomics *73*, 56–65.

Lehman, J.J., Barger, P.M., Kovacs, A., Saffitz, J.E., Medeiros, D.M., and Kelly, D.P. (2000). Peroxisome proliferator-activated receptor gamma coactivator-1 promotes cardiac mitochondrial biogenesis. J. Clin. Invest. *106*, 847–856.

Li, C., and Wong, W.H. (2001). Model-based analysis of oligonucleotide arrays: expression index computation and outlier detection. Proc. Natl. Acad. Sci. USA *98*, 31–36.

Lillioja, S., Mott, D.M., Howard, B.V., Bennett, P.W., Yki-Jarvinen, H., Freymond, D., Nyomba, B.L., Zurlo, F., Swinburn, B., and Bogardus, C. (1988). Impaired glucose tolerance as a disorder of insulin action. Longitudinal and cross-sectional studies in Pima Indians. N. Engl. J. Med. *318*, 1217–1225.

Lillioja, S., Mott, D.M., Spraul, M., Ferraro, R., Foley, J.E., Ravussin, E., Knowler, W.C., Bennett, P.W., and Bogardus, C. (1993). Insulin resistance and insulin secretory dysfunction as precursors of non-insulin-dependent diabetes mellitus. Prospective studies of Pima Indians. N. Engl. J. Med. *329*, 1988–1992.

Lin, J., Puigserver, P., Donovan, J., Tarr, P., and Spiegelman, B.M. (2002a). Peroxisome proliferator activated receptor γ coactivator 1β (PGC-1β), a novel PGC-1 related transcription coactivator associated with host cell factor. J. Biol. Chem. *277*, 1645–1648.

Lin, J., Wu, H., Zhang, C.Y., Wu, Z., Boss, O., Michael, L.F., Puigserver, P., Isotani, E., Olson, E.N., Lowell, B.B., et al. (2002b). Transcriptional co-activator PGC-1α drives the formation of slow-twitch muscle fibres. Nature *428*, 797–801.

Lin, J., Tarr, P., Yang, R., Rhee, J., Puigserver, P., Newgard, C.B., and Spiegelman, B.M. (2003). PGC-1beta in the regulation of hepatic glucose and energy metabolism. J. Biol. Chem. *278*, 30843–30848.

Lin, J., Yang, R., Tarr, P.T., Wu, P.H., Pei, L., Uldry, M., Tontonoz, P., Newgard, C.B., and Spiegelman, B.M. (2005). Hyperlipidemic effects of dietary saturated fats mediated through PGC-1β coactivation of SREBP. Cell *120*, 261–273.

Lowell, B.B., and Shulman, G.I. (2005). Mitochondrial dysfunction and type 2 diabetes. Science *307*, 384–387.

Meirhaeghe, A., Crowley, V., Lenaghan, C., Lelliott, C., Green, K., Stewart, A., Hart, K., Schinner, S., Sethi, J.K., Yeo, G., et al. (2003). Characterization of the human, mouse and rat PGC-1β (peroxisome proliferator activated receptor γ coactivator 1β) gene *in vitro* and *in vivo*. Biochem. J. *373*, 155–165.

Michael, L.F., Wu, Z., Cheatham, R.B., Puigserver, P., Adelmant, G., Lehman, J.J., Kelly, D.P., and Spiegelman, B.M. (2001). Restoration of insulin-sensitive glucose transporter (GLUT4) gene expression in muscle cells by the transcriptional coactivator PGC-1. Proc. Natl. Acad. Sci. USA *98*, 3820–3825.

Mootha, V.K., Lindgren, C.M., Eriksson, K.F., Subramanian, A., Sihag, S., Lehar, J., Puigserver, P., Carlsson, E., Ridderstrale, M., Laurila, E., et al. (2003). PGC1-α responsive genes involved in oxidative phosphorylation are coordinately downregulated in human diabetes. Nat. Med. *34*, 267–273.

Mootha, V.K., Handschin, C., Arlow, D., Xie, X., St-Pierre, J., Sihag, S., Yang, W., Altshuler, D., Puigserver, P., Patterson, N., et al. (2004). ERRα and Gabpa/b specify PGC1α-dependent oxidative phosphorylation gene expression that is altered in diabetic muscle. Proc. Natl. Acad. Sci. USA *101*, 6570–6575.

Morino, K., Petersen, K.F., Dufour, S., Befroy, D., Frattini, J., Shatzkes, N., Neschen, S., White, M.F., Bilz, S., Sono, S., et al. (2005). Reduced mitochondrial density and increased IRS-1 serine phosphorylation in muscle of insulin-resistant offspring of type 2 diabetic parents. J. Clin. Invest. *115*, 3587–3593.

Neschen, S., Morino, K., Hammond, L.E., Zhang, D., Liu, Z.X., Romanelli, A.J., Cline, G.W., Pongratz, R.L., Zhang, X.M., Choi, C.S., et al. (2005). Prevention of hepatic steatosis and hepatic insulin resistance in mitochondrial acyl-CoA:glycerol-sn-3-phosphate acyltransferase 1 knockout mice. Cell Metab. *2*, 55–65.

Patti, M.E., Butte, A.J., Crunkhorn, S., Cusi, K., Berria, R., Kashyap, S., Miyazaki, Y., Kohane, I., Costello, M., Saccone, R., et al. (2003). Coordinated reduction of genes of oxidative metabolism in humans with insulin resistance and diabetes: Potential role of *PGC1* and *NRF1*. Proc. Natl. Acad. Sci. USA *100*, 8466–8471.

Petersen, K.F., Befroy, D., Dufour, S., Dziura, J., Ariyan, C., Rothman, D.L., DiPietro, L., Cline, G.W., and Shulman, G.I. (2003). Mitochondrial dysfunction in the elderly: possible role in insulin resistance. Science *300*, 1140–1142.

Petersen, K.F., Dufour, S., Befroy, D., Garcia, R., and Shulman, G.I. (2004). Impaired mitochondrial activity in the insulin-resistant offspring of patients with type 2 diabetes. N. Engl. J. Med. *350*, 664–671.

Puigserver, P., and Spiegelman, B.M. (2003). Peroxisome proliferator-activated receptor γ coactivator 1α (PGC1α): transcriptional coactivator and metabolic regulator. Endocr. Rev. *24*, 78–90.

Ritov, V.B., Menshikova, E.V., He, J., Ferrell, R.E., Goodpaster, B.H., and Kelley, D.K. (2005). Deficiency of subsarcolemmal mitochondria in obesity and type 2 diabetes. Diabetes *54*, 8–14.

Rustin, P., Chretien, D., Bourgeron, T., Gérard, B., Rötig, A., Saudubray, J.M., and Munnich, A. (1994). Biochemical and molecular investigations in respiratory chain deficiencies. Clin. Chim. Acta *228*, 35–51.

Samuel, V.T., Liu, Z.X., Qu, X., Elder, B.D., Bilz, S., Befroy, D., Romanelli, A.J., and Shulman, G.I. (2004). Mechanism of hepatic insulin resistance in nonalcoholic fatty liver disease. J. Biol. Chem. *279*, 32345–32353.

Savkur, R.S., and Burris, T.P. (2004). The coactivator LXXLL nuclear receptor recognition motif. J. Pept. Res. *63*, 207–212.

Schreiber, S.N., Emter, R., Hock, M.B., Knutti, D., Cardenas, J., Podvinec, M., Oakeley, E.J., and Kralli, A. (2004). The estrogen-related receptor α (ERRα) functions in PPARγ coactivator 1α (PGC-1α)-induced mitochondrial biogenesis. Proc. Natl. Acad. Sci. USA *101*, 6472–6477.

Shulman, G.I. (2000). Cellular mechanisms of insulin resistance. J. Clin. Invest. *106*, 171–176.

St-Pierre, J., Lin, J., Krauss, S., Tarr, P.T., Yang, R., Newgard, C.B., and Spiegelman, B.M. (2003). Bioenergetic analysis of peroxisome proliferator-activated receptor-γ coactivators 1α and 1β (PGC-1α and PGC-1β) in muscle cells. J. Biol. Chem. *278*, 26597–26603.

Warram, J.H., Martin, B.C., Krolewski, A.S., Soeldner, J.S., and Kahn, C.R. (1990). Slow glucose removal rate and hyperinsulinemia precede the development of type II diabetes in the offsprings of diabetic patients. Ann. Intern. Med. *113*, 909–915.

Wolfrum, C., and Stoffel, M. (2006). Coactivation of Foxa2 through Pgc-1β promotes liver fatty acid oxidation and triglyceride/VLDL secretion. Cell Metab. *3*, 99–110.

Wu, Z., Puigserver, P., Andersson, U., Zhang, C.Y., Adelmant, G., Mootha, V., Troy, A., Cinti, S., Lowell, B., Scarpulla, R.C., and Spiegelman, B.M.

(1999). Mechanisms controlling mitochondrial biogenesis and respiration through the thermogenic coactivator PGC-1. Cell *98*, 115–124.

Youn, J.H., and Buchanan, T.A. (1993). Fasting does not impair insulin-stimulated glucose uptake but alters intracellular glucose metabolism in conscious rats. Diabetes *42*, 757–763.

Yu, C., Chen, Y., Cline, G.W., Zhang, D., Zong, H., Wang, Y., Bergeron, R., Kim, J.K., Cushman, S.W., Cooney, G.J., et al. (2002). Mechanism by which fatty acids inhibit insulin activation of IRS-1 associated phosphatidylinositol 3-kinase activity in muscle. J. Biol. Chem. *277*, 50230–50236.

Zimmet, P., Alberti, K.G.M.M., and Shaw, J. (2001). Global and societal implications of the diabetes epidemic. Nature *414*, 782–787.

Accession numbers

The Affymetrix GeneChip data set is publicly available from the Gene Expression Omnibus (GEO; http://www.ncbi.nlm.nih.gov/geo/) with the accession number GSE6210.